Geochemical Perspectives Letters

Geochemical evolution of melt/peridotite interaction at high pressure in subduction zones

N. Malaspina[1*], G. Borghini[2], S. Zanchetta[1], L. Pellegrino[1], M. Corti[1], S. Tumiati[2]

OPEN ACCESS

https://doi.org/10.7185/geochemlet.2305

Abstract

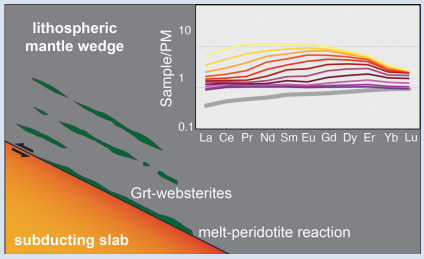

The Borgo outcrop of the Monte Duria Area (Adula-Cima Lunga unit, Central Alps, Italy) is an excellent example of melt-peridotite interaction which occurred under a deformation regime at high pressure, that enabled the combination of porous and focused flow of eclogite-derived melts into garnet peridotites. Migmatised eclogites are in direct contact with retrogressed garnet peridotites and the contact is marked by a tremolitite layer, also occurring as boudins parallel to the garnet layering in the peridotites, derived from a garnet websterite precursor produced by the interaction between eclogite-derived melts with the peridotite at high pressure. LREE concentrations of tremolitite along a 120 m length profile, starting from the eclogite-peridotite contact to the inner part of the peridotite, show a progressive enrichment coupled with a peculiar fractionation. Numerical modelling assuming the eclogitic leucosome as the starting percolating melt reproduces the REE enrichment and LREE/HREE fractionation observed in tremolitite bulk rocks within the first 30 m. The comparison between the REE composition of the retrogressed garnet websterites along the profile and the result of our model suggests that reactive melt infiltration at high pressure is a plausible mechanism to modify the REE budget of mantle peridotites that lie on top of the subducting crustal slab.

Received 15 June 2022 | Accepted 22 January 2023 | Published 10 February 2023

Introduction and Petrological Background

The fate of crust-derived melts at warm subduction zones and the transport mechanism of slab-derived components to the supra-subduction mantle is still a matter of debate. Some natural occurrences show that the migration of crust-derived melts into the mantle by porous flow is limited by instant reaction with the peridotites and the consequent production of metasomatic orthopyroxene (±clinopyroxene) and phlogopite hybrid rocks at the slab-mantle interface (*e.g.*, Malaspina *et al.*, 2006; Vrijmoed *et al.*, 2013; Endo *et al.*, 2015). Alternatively, the occurrence of a network of pyroxenite veins in metasomatised mantle xenoliths from arc lavas indicates that metasomatic melts may percolate the mantle by a mechanism of focused flow (*e.g.*, Kepezhinskas *et al.*, 1995; Arai *et al.*, 2003). Melt-peridotite interaction *via* reactive porous flow has been largely studied in mantle samples from oceanic and subcontinental settings (*e.g.*, Godard *et al.*, 1995; Ionov *et al.*, 2005; Borghini *et al.*, 2020). In comparison, we know little about the role of these interactions at high pressure (HP) and relatively low temperature (LT) such as those reached at the slab interface, even in warm subduction zones (*e.g.*, Malaspina *et al.*, 2006; Scambelluri *et al.*, 2006; Pellegrino *et al.*, 2020).

The Borgo outcrop of the Monte Duria area (Adula-Cima Lunga unit, Central Alps, Italy) is an ideal example of melt-peridotite interaction which occurred under a deformation regime at HP, that enabled the combination of porous and focused flow of eclogite-derived melts into Grt-peridotites (Pellegrino *et al.*, 2020; mineral abbreviations from Warr, 2021). In the Monte Duria area Grt-peridotites occur in direct contact with migmatised orthogneiss (Mt. Duria) and eclogites (Borgo). Both eclogites and peridotites record a common HP peak at 2.8 GPa and 750 °C and post-peak high temperature (HT) equilibration at 0.8–1.0 GPa and 850 °C (Tumiati *et al.*, 2018). Grt-peridotites show metasomatic pargasitic to edenitic amphibole, dolomite, phlogopite and orthopyroxene after olivine, crystallised after the interaction with crust-derived agents enriched in SiO_2, K_2O, CO_2 and H_2O at peak conditions (Tumiati *et al.*, 2018; Pellegrino *et al.*, 2020). They also show a "spoon-shape" fractionation in LREE ($La_N/Nd_N = 2.4$) related to the LREE enrichment in clinopyroxene and amphibole crystallised in the garnet stability field, interpreted by Pellegrino *et al.* (2020) as acquired by the interaction with a hydrous melt.

At Borgo, migmatised eclogites are in direct contact with retrogressed Grt-peridotites showing a garnet compositional layering, cross cut by a subsequent low pressure (LP) chlorite foliation (Pellegrino *et al.*, 2020). Eclogite boudins enclosed in migmatites show thin films and interstitial pockets of crystallised melts parallel to the eclogite foliation, indicating that partial melting of eclogites occurred at HP conditions (Pellegrino *et al.*, 2020). Tremolitites occur both at the peridotite/eclogite contact and within the peridotite body and derived from the retrogression of previous Grt-websterites formed after the interaction at HP between eclogite-sourced melts and peridotites (Pellegrino *et al.*,

1. Department of Earth and Environmental Sciences, Università degli Studi di Milano-Bicocca, Piazza della Scienza 4, I-20126 Milano, Italy
2. Department of Earth Sciences, Università degli Studi di Milano, Via Botticelli 23, I-20133 Milano, Italy
* Corresponding author (email: nadia.malaspina@unimib.it)

2020). Both peridotites and tremolitites record a LREE enrichment acquired during the melt/peridotite interaction at HP, decoupled by the selective enrichment in large ion lithophile elements (LILE) acquired by late stage tremolitic hornblende and tremolite crystallisation during a hydration event at LP conditions (Pellegrino *et al.*, 2020). This fluid-assisted event led to the formation of a chlorite foliation post-dating the garnet layering in peridotites, and the retrogression of Grt-websterites into tremolitites (Fig. 1a).

In this work we aim to resolve the role of melt/peridotite interaction at HP conditions in the selective REE transfer from a proxy of subducting slab (eclogitic migmatite) to the overlying mantle (associated retrogressed Grt-peridotite). Percolative reactive flow at decreasing melt/mass and high instantaneous melt/peridotite ratios, combined with moderate extents of fractional crystallisation of the resulting melt (retrogressed Grt-websterites), accounts for an overall REE enrichment and LREE/HREE fractionation observed in the natural example of the Borgo outcrop.

Field Description and Geochemistry

Tremolitites and Phl-bearing tremolitites occur as bright green layers, a few centimetres up to several tens of cm thick, at the

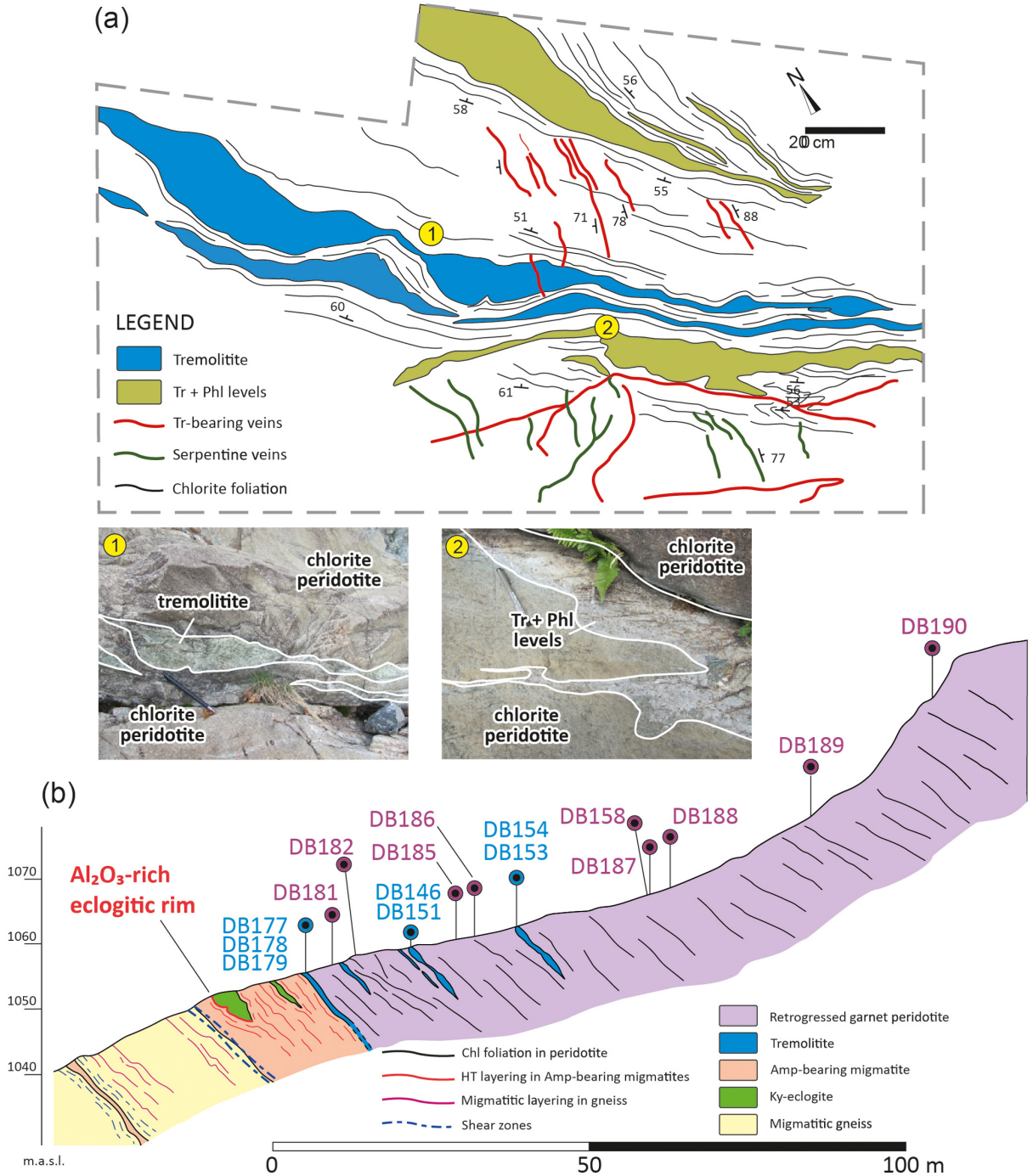

Figure 1 **(a)** Geological sketch map of tremolitite layers in retrogressed Grt-peridotite at the contact with migmatitic eclogites. (1) Tremolitite showing sharp contact with the host retrogressed Grt-peridotite. (2) Tr + Phl layer displaying a diffusive contact with retrogressed Grt-peridotite. **(b)** Cross section of the peridotite host rock contact with sampling location of tremolitites and Chl-peridotites.

eclogite/peridotite contact and within the peridotite, displaying a boudinage (Fig. 1). The peridotite Grt-layering flows into the necks of the boudins, indicating that the stretching of the tremolitites (previous Grt-websterite) occurred when the peridotites were still in the garnet stability field. A detailed microstructural description is reported in the Supplementary Information (Fig. S-1, Table S-1 and S-2).

We analysed the major and trace element composition of 16 samples (Table S-3) collected along a profile of about 120 m, starting from the eclogite-peridotite contact to the inner part of the peridotite lens (Fig. 1b, Table S-1). As shown in Figure S-2a, the composition of Chl-peridotites displays Mg# (90), high Ni (2097–2518 μg/g), and low Al_2O_3 (0.77–3.50 wt. %) and CaO (0.62–2.60 wt. %) concentrations. Tremolitites show high Mg# (0.91) and Ni (up to 1390 μg/g) plotting into the field of the ultramafic compositions in the Mg#-Ni variation diagram, with a marked difference with respect to Grt- and Spl-pyroxenites of subcontinental ophiolites (*e.g.*, External Ligurides ophiolites; Montanini *et al.*, 2012). The Al_2O_3 concentrations are comparable to mantle values (Table S-3, Fig. S-2b), but they show high SiO_2 (up to 57.50 wt. %), high CaO (up to 13.34 wt. %) and Al_2O_3 *versus* SiO_2/MgO (Fig. S-2b) close to the composition of metasomatic Grt-orthopyroxenites and websterites from Dabie-Shan, which were formed after the interaction of Grt-harzburgites with Si-rich crust-derived melts at UHP (Malaspina *et al.*, 2006).

The bulk rock trace element compositions of the analysed peridotites and tremolitites are portrayed in Figure S-3, normalised to the Primitive Mantle (PM). The trace element patterns of the Depleted MORB Mantle (DMM; Salters and Stracke, 2004), of Grt-peridotites from Mt. Duria (same area as Borgo) and the REE patterns of subcontinental Grt-pyroxenites from the External Ligurides are also reported for comparison. Peridotites show REE concentrations close to or slightly lower than the DMM, with fractionated patterns enriched in LREE (La_N/Nd_N up to 1.07) relative to the MREE and HREE (Fig. S-3a). Tremolitites have REE concentrations up to 4.63 × PM with enrichments in MREE and LREE/HREE two orders of magnitude higher than subcontinental pyroxenites from External Ligurides (Fig. S-3b). Both peridotites close to the contact with the migmatised eclogites, and tremolitites display a negative Eu anomaly, resembling that of eclogite leucosome (dark diamonds in Figs. 2, S-3) produced from a Pl-bearing source. In terms of other trace elements, Chl-peridotites and tremolitites show similar LILE patterns and fluid immobile element (Nb, Zr, Hf) concentrations (Table S-3 and Fig. S-3c,d). Among the fluid mobile elements, the selective enrichment in LILE recorded by the peridotites and tremolitites (Fig. S-3c) resembles that of retrograde tremolitic hornblende, chlorite and tremolite reported by Pellegrino *et al.* (2020), indicating that a fluid-mediated metasomatism occurred at LP conditions.

REE Geochemical Evolution in Grt-websterites and Peridotites at HP

Figure S-4 portrays selected REE (La, Ce, Sm, Yb) and fluid mobile elements (Sr) of peridotites and tremolitites along a 120 m long profile from the migmatised eclogite-peridotite contact (0 m) to the innermost part of the peridotite lens (Fig. 1). Tremolitites show a progressive increase in LREE abundances from the contact up to about 30 m within the adjacent peridotite (Fig. S-4a-c). Among the fluid mobile elements, both tremolitites and peridotites show a progressive depletion in Pb from the contact to 80 m within the peridotite body (Fig. S-3c,d), whereas Sr is almost constant (Fig. S-4e). As demonstrated by Pellegrino *et al.* (2020), the LREE enrichment and fractionation of the peridotites was most likely generated by the infiltration and interaction at HP of the eclogite-derived melt (leading to the emplacement of pristine Grt-websterites), rather than to the LP fluid-assisted metasomatic event that led to the retrogression of Grt-peridotites and websterites into Chl-peridotites and tremolitites, respectively. The reactive percolation of the eclogite-derived melt through the peridotite may be, in turn, responsible for the LREE-HREE fractionation (Ce/Yb), observed in the retrogressed Grt-websterite (now tremolitite) bulk rocks within the first 30 m of peridotite (Figs. 2, S-3; normalisation values are from McDonough and Sun (1995).

To test this hypothesis, we have numerically simulated the REE gradient applying the Plate Model of Vernieres *et al.* (1997) using the REE composition of the eclogite leucosome of Pellegrino *et al.* (2020) as starting melt and the DMM as peridotite matrix. In the first step (Fig. 2a), the crustal melt derived from partial melting of eclogites (black diamonds) reacts with the

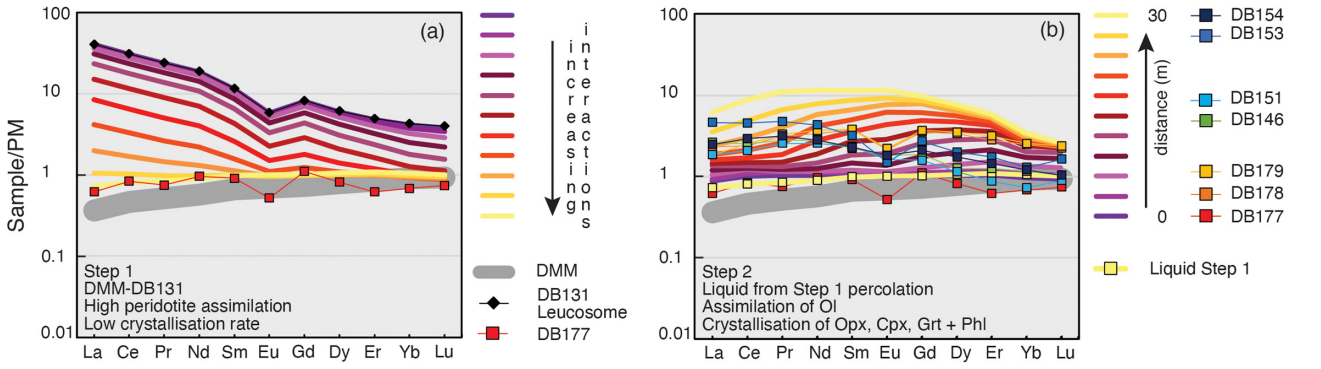

Figure 2 Numerical simulation of melt-rock interaction at peridotite-eclogite interface and reactive percolation of melt through mantle peridotite **(a)** PM normalised REE patterns of liquids resulting from interaction between mantle peridotite and the initial liquid, assuming high peridotite assimilation (60 % Ol, 20 % Opx, 12 % Cpx, 3 % Grt) and low crystallisation rate (60 % Cpx, 40 % Grt). After 11 interactions, we obtained a pattern that reproduces the LREE/HREE bulk composition of retrogressed Grt-websterite at the mantle-eclogite boundary, *i.e.* distance 0 in the profile of Figure 1. **(b)** Evolution of PM normalised REEs in the liquid originated by reactive percolation of reacted melt after Step 1 through the DMM peridotite. The model assumes a high infiltrating melt amount, low assimilation of olivine and high extent of crystallisation. Patterns with coloured squares (except light yellow) are the REE bulk compositions of tremolitites sampled in the Borgo outcrop within the first 30 metres from the migmatitic eclogite-peridotite contact (Figs. 1, S-1). Coloured lines refer to the progressive cells of the model. See the Supplementary Information for details of input parameters and further explanation.

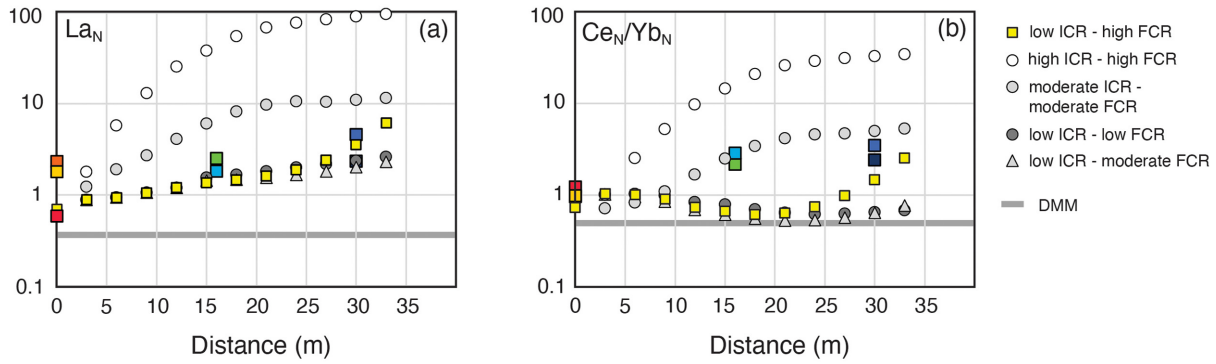

Figure 3 PM normalised La and Ce/Yb of tremolitite (same symbols as Fig. 2) along the section of Figure 1, compared to the results of the numerical simulation of reactive melt percolation assuming variable crystallisation rate of Opx, Cpx, Grt and Phl. ICR and FCR are Initial and Final Crystallisation Rate. Yellow symbols represent the preferred model. The grey line is the reference DMM.

peridotite (grey line) at the eclogite-peridotite interface. The liquids resulting from increasing interactions (violet to yellow lines of Fig. 2a) are assumed to form veins of websterites (see also Fig. S-5) that are supposed to be the protoliths of tremolitites preserving their original REE composition. After several interactions, the final reacted melt crystallised at the eclogite-peridotite contact likely forms the first websterite DB177, showing a diffusive contact with retrogressed Grt-peridotite (Figs. 1a, 2a). Notably, we obtain a comparable result by using an adakitic melt (*adakite*2 from Corgne *et al.*, 2018), as starting melt (see Fig. S-6a). After the interaction at the eclogite-peridotite contact, the reacted melt infiltrates the peridotite producing the REE gradient observed in the tremolitites profile. We assume an initial peridotite porosity of 20 % (Fig. S-6b) that reflects a high peridotite assimilation coupled with the progressive melt consumption through melt-peridotite reaction during the percolation (*i.e.* a high extent of transient melt crystallisation), simulated by the progressive increase in crystallisation rate of 50 % Opx, 20 % Cpx, 20 % Grt, 10 % Phl (Figs. 2b, S-5). Figure 3 reports the La_N and Ce_N/Yb_N resulting from Step 2 calculations (yellow squares) compared with those measured in our tremolitite (coloured squares) along the first 30 m from the eclogite-peridotite contact. Grey scale symbols show the sensitivity of the model to the different extents of initial and final crystallisation rate of the percolating melts in the fractionation of LREE/HREE.

The numerical simulation aims to model the effect of interaction between crust-derived melts produced by partial melting of mafic components of the slab with the supra-subduction mantle peridotite at sub-arc depths (3 GPa, 750 °C). This includes a first step of crustal magma stagnation and melt-peridotite reaction at the slab-mantle interface and the following metre-scale percolation of reacted melt within the overlying peridotite that buffers the composition of the infiltrating melt. The comparison between the REE composition of the retrogressed Grt-websterites along the profile and the result of our model suggests that reactive melt infiltration at HP is a plausible mechanism to modify the REE budged of mantle peridotites that lie on top of the subducting crustal slab. Samples from those settings tend to show peculiar LREE "spoon-like" fractionations (*e.g.*, Scambelluri *et al.*, 2006). Moreover, the melt/peridotite interaction and the percolation of slab-derived melts into the overlying mantle may strongly modify the overall REE abundance and LREE/HREE fractionation (*e.g.*, Ce_N/Yb_N) of the residual crustal melt within the first 30 m of slab/mantle interface.

Acknowledgements

We thank C. Prigent and J.C.Vrijimoed for constructive reviews and H.R. Marschall for editorial handling. This work was funded by the Italian Ministry of University and Research (PRIN 2017 - Prot. 2017ZE49E7_005 - The Dynamic Mass Transfer from Slabs to Arcs).

Editor: Horst R. Marschall

Additional Information

Supplementary Information accompanies this letter at https://www.geochemicalperspectivesletters.org/article2305.

Cite this letter as: Malaspina, N., Borghini, G., Zanchetta, S., Pellegrino, L., Corti, M., Tumiati, S. (2023) Geochemical evolution of melt/peridotite interaction at high pressure in subduction zones. *Geochem. Persp. Let.* 24, 48–52. https://doi.org/10.7185/geochemlet.2305

References

Arai, S., Ishimaru, S., Okrugin, V.M. (2003) Metasomatized harzburgite xenoliths from Avacha volcano as fragments of mantle wedge of the Kamchatka arc: implication for the metasomatic agent. *Island Arc* 12, 233–246. https://doi.org/10.1046/j.1440-1738.2003.00392.x

Borghini, G., Rampone, E., Zanetti, A., Class, C., Fumagalli, P., Godard, M. (2020) Ligurian pyroxenite-peridotite sequences (Italy) and the role of melt-rock reaction in creating enriched-MORB mantle sources. *Chemical Geology* 532, 119252. https://doi.org/10.1093/petrology/egv031

Corgne, A., Schilling, M.E., Grégoire, M., Langlade, J. (2018). Experimental constraints on metasomatism of mantle wedge peridotites by hybridized adakitic melts. *Lithos,* 308, 213–226. https://doi.org/10.1016/j.lithos.2018.03.006

Endo, S., Mizukami, T., Wallis, S.R., Tamura, A., Arai, S. (2015) Orthopyroxene-rich rocks from the sanbagawa belt (SW Japan): fluid–rock interaction in the forearc slab– mantle wedge Interface. *Journal of Petrology* 56, 1113–1137. https://doi.org/10.1093/petrology/egv031

Godard, M., Bodinier, J.L., Vasseur, G. (1995) Effects of mineralogical reactions on trace element redistributions in mantle rocks during percolation processes: a chromato- graphic approach. *Earth and Planetary Science Letters* 133, 449–461. https://doi.org/10.1016/0012-821X(95)00104-K

Ionov, D.A., Chanefo, I., Bodinier, J.L. (2005) Origin of Fe-rich lherzolites and wehrlites from Tok, SE Siberia by reactive melt per- colation in refractory mantle peridotites. *Contributions to Mineralogy and Petrology* 150, 335–353. https://doi.org/10.1007/s00410-005-0026-7

Kepezhinskas, P.K., Defant, M.J., Drummond, M.S. (1995) Na metasomatism in the island-arc mantle by slab melt—peridotite interaction: evidence from mantle xenoliths in the North Kamchatka Arc. *Journal of Petrology*, 36, 1505–1527. https://doi.org/10.1093/oxfordjournals.petrology.a037263

Malaspina, N., Hermann, J., Scambelluri, M., Compagnoni, R. (2006) Polyphase inclusions in garnet-orthopyroxenite (Dabie-Shan, China) as monitors for metasomatism and fluid-related trace element transfer in subduction zone peridotite. *Earth and Planetary Science Letters* 249, 173–187. https://doi.org/10.1016/j.epsl.2006.07.017

McDonough, W.F., Sun, S.S. (1995) Composition of the Earth. *Chemical Geology* 120, 223–253. https://doi.org/10.1016/0009-2541(94)00140-4

Montanini, A., Tribuzio, R., Thirlwall, M. (2012) Garnet clinopyroxenite layers from the mantle sequences of the Northern Apennine ophiolites (Italy): Evidence for recycling of crustal material. *Earth and Planetary Science Letters* 351-352, 171–181. https://doi.org/10.1016/j.epsl.2012.07.033

Pellegrino, L., Malaspina, N., Zanchetta, S., Langone, A., Tumiati, S. (2020) High pressure melting of eclogites and metasomatism of garnet peridotites from Monte Duria Area (Central Alps, N Italy): A proxy for melt-rock reaction during subduction. *Lithos* 358-359, 105391. https://doi.org/10.1016/j.lithos.2020.105391

Salters, V.J.M., Stracke, A. (2004) Composition of the depleted mantle. *Geochemistry Geophysics Geosystems* 5. https://doi.org/10.1029/2003GC000597

Scambelluri, M., Hermann, J., Morten, L., Rampone, E. (2006) Melt-versus fluid-induced metasomatism in spinel to garnet wedge peridotites (Ulten Zone, Eastern Italian Alps): Clues from trace element and Li abundances. *Contributions to Mineralogy and Petrology* 151, 372–394. https://doi.org/10.1007/s00410-006-0064-9

Tumiati, S., Zanchetta, S., Pellegrino, L., Ferrario, C., Casartelli, S., Malaspina, N. (2018) Granulite-facies overprint in garnet peridotites and kyanite eclogites of Monte Duria (Central Alps, Italy): clues from srilankite-and sapphirine-bearing symplectites. *Journal of Petrology* 59, 115–151. https://doi.org/10.1093/petrology/egy021

Vernieres, J., Godard, M., Bodinier, J.L. (1997) A plate model for the simulation of trace element fractionation during partial melting and magma transport in the Earth's upper mantle. *Journal of Geophysical Research* 102, 24771–24784. https://doi.org/10.1029/97JB01946

Vrijmoed, J.C., Austrheim, H., John, T., Hin, R.C., Corfu, F., Davies, G.R. (2013) Metasomatism in the ultrahigh-pressure Svartberget garnet-peridotite (Western Gneiss Region, Norway): implications for the transport of crust-derived fluids within the mantle. *Journal of Petrology* 54, 1815–1848. https://doi.org/10.1029/97JB01946

Warr, L.N. (2021) IMA–CNMNC approved mineral symbols. *Mineralogical Magazine* 85, 291–320. https://doi.org/10.1180/mgm.2021.43

Geochemical Perspectives Letters

Geochemical evolution of melt/peridotite interaction at high pressure in subduction zones

N. Malaspina, G. Borghini, S. Zanchetta, L. Pellegrino, M. Corti, S. Tumiati,

Supplementary Information

The Supplementary Information includes:

- S. 1 Microstructural Description of Peridotites and Websterite-Tremolitite of the Borgo outcrop
- S. 2 Analytical Techniques
- S. 3 Geochemical Modelling
- S. 4 Thermodynamic Modelling
- Tables S-1 to S-3
- Figures S-1 to S-6
- Supplementary Information References

S. 1 Microstructural Description of Peridotites and Websterite-Tremolitite of the Borgo Outcrop

Chl-peridotites show a porphyroclastic structure (Fig. S-1a) characterised by coarse olivine (Ol_1), orthopyroxene (Opx_1), rarely preserved clinopyroxene (Cpx_1) and garnet completely substituted by chlorite (Chl_1; Fig. S-1b) during a HP hydration event that crystallised relict pargasitic to edenitic amphibole (Amp_1) and yielded to the partial melting of the associated eclogites (see Pellegrino *et al*., 2020). The interaction with eclogite-sourced melts and the Grt-Chl-peridotite at HP produced a porphyroblastic assemblage made of poikilitic orthopyroxene (Opx_{porph}) including Ol_1 (Fig. S-1c), amphibole (Amp_{porph}) and phlogopite (Phl_{porph}) postdating the original Grt-peridotite assemblage. Thermodynamic modelling indicates that the interaction between the eclogitic melt, and the surrounding Grt-Chl-peridotite likely produced layers of Grt-websterites (now retrogressed into tremolitites) constituted by Opx, Cpx, Grt and Hbl (Pellegrino *et al*., 2020). The first stage of decompression produced a finer grained recrystallised matrix of Ol_2, Opx_2, pargasitic to edenitic amphibole (Amp_2) and spinel (Spl_2) in the peridotites (Fig. S-1d) and crystallised Hbl in the Grt-websterites (Fig. S-1e).

After the decompression, a LP-(U)HT event has been recorded by Grt-peridotites of Mt. Duria and Borgo eclogites, with crystallisation of symplectitic Opx_{sym}, Cpx_{sym}, pargasitic Amp_{sym}, Sp_{sym}, Spr + Bdy + Sri around garnet in the peridotites (Tumiati *et al*. 2018) and Spr+Crn around kyanite in the eclogites (Tumiati *et al*. 2018). In those samples of Borgo peridotites close to the contact with the eclogitic migmatite, chlorite (Chl_3) and tremolitic to edenitic amphibole (Amp_3) are aligned along a pervasive foliation (Fig. S-1d), indicative of a late-stage LP-LT hydration event, that

substitute all the previous mineral parageneses. This hydration event transformed the Grt-websterites into tremolitites, showing relict of coarse Mg-hornblende (Hbl), surrounded by a fine-grained and mosaic like matrix of tremolite (Tr_1) overgrown by a second generation of mm-sized Tr_2 (Fig. S-1e). The samples closed to the contact between eclogitic migmatite and Chl-peridotite show Tr + Phl + Tlc + Chl pseudomorphs after garnet (Fig. S-1f). A summary of the mineral parageneses reconstructed in Chl-peridotites and tremolitites is reported in Table S-2.

S. 2 Analytical Techniques

Major and trace elements whole-rock analyses were performed by inductively coupled plasma mass spectrometry (ICP-MS) and LECO combustion (total C, S) at Bureau Veritas ACME Mineral Laboratories, Canada. Results are reported in Table S-3.

S. 3 Geochemical Modelling

We use the "Plate Model" proposed by Vernières *et al*. (1997) to simulate the REE gradient shown by the tremolitite veins sampled within the first 30 meters of peridotite from the eclogite-peridotite contact (see profile in Fig. 1). The numerical simulation reproduces a rock-dominated system where the solid matrix, varying in porosity and in modal composition along the percolation column, buffers the composition of the infiltrating melt. In our case, the profile through the peridotites containing the tremolitite veins represents the mantle column that we ideally divide in meter-scale portions ("cells") of peridotite infiltrated by the same melts. Note that the cell-1 is adjacent to the source of infiltrating melt, *i.e*., peridotite-eclogite interface, whereas the number of cells increases going furthest away. The composition of liquids resulting from calculation is here assumed to form veins of Grt-websterites (see also thermodynamic modelling) that are therefore the protoliths of tremolitites that still preserve their original bulk REE composition. We approximate the REE composition of liquid to the REE abundance of pyroxenites embedded in Borgo peridotite at variable distance from the eclogite-peridotite contact.

The initial solid matrix is the DMM of Salters and Stracke (2004) having a Grt-lherzolite mode of Ol:Opx:Cpx:Grt = 0.60:0.25:0.12:0.03. The REE compositions of olivine, orthopyroxene, clinopyroxene and garnet are calculated assuming equilibrium with the REE composition of DMM, using partition coefficients by Salters *et al*. (2002). Normalising values are from McDonough and Sun (1995). Our model assumes the eclogite-derived leucosome DB131 composition (Pellegrino *et al*., 2020) as starting percolating melt.

The geochemical model includes two steps of melt-peridotite reaction: *first step* (Step1) assumes high peridotite assimilation step (*i.e.,* high M_a/M_c ratio, where M_a is the mass of assimilated peridotite and M_c is the mass of crystallised melt) at crust-mantle boundary and it is followed by a *second step* (Step2) of reacted melt percolation within the adjacent peridotite assuming variable amounts of olivine assimilation and pyroxene + garnet (+ amphibole or phlogopite) crystallisation. The *first step* (Step1) simulates the interaction of eclogite-derived melt (DB131) with peridotite (DMM) at the peridotite-eclogite interface, assuming an initial porosity of 0.1 in the peridotite, high extent of peridotite assimilation and low rate of clinopyroxene + garnet crystallisation (0.6 and 0.4 respectively). This step generates a final liquid with REE composition that well reproduces the pyroxenite vein DB177 sampled at the eclogite-peridotite contact (see Fig. 2a). We obtained a comparable result by replicating the calculation using the *adakite2* from Corgne *et al*. (2018), as initial reacting melt (Fig. S-6a). Although garnet and clinopyroxene are the main minerals expected to crystallize from an eclogite-derived melt at about 2 GPa (Pertermann and Hirschmann, 2003; Wang *et al*., 2020), orthopyroxene can be also precipitated as a result of reaction with the peridotite (Rapp *et al*., 2010, Wang *et al*., 2020; see also Fig. S-5). Nevertheless, the model shows that at high M_a/M_c ratio the addition of variable amount (30 or 50%) of orthopyroxene (having rather low K_d for the REEs) in the crystallizing assemblage does not impact significantly on the melt REE composition resulting from the reaction (Fig.S-6b). We also evaluated the role of variable extent of initial porosity: Figure S-6b shows that porosity higher than 0.1 fails to reproduce the low La_N/Sm_N of melt that generated the

retrogressed Grt-websterite (DB177) close to the contact with the peridotite-eclogite interface. On contrary, assuming porosity lower than 0.1 the model results in too fast melt La_N/Sm_N lowering.
In the *second step* (Step2), our model simulates the reactive melt percolation through the first 36 meters of peridotite from the crust-mantle contact as described in the profile of Figure 1b. We assume a relatively high instantaneous melt/peridotite ratio (*i.e.*, initial porosity of 0.2, which reflects the high peridotite assimilation of the Step1; Fig. S-6b) combined with high extents of fractional crystallisation and very low mass assimilation (M_a/M_c ratio of 0.56-0.61), which result in a rapid decrease of melt mass at increasing interaction cells. The choice of this combination of parameters is justified by a scenario of reactive melt percolation from a melt source at slab-mantle interface, explaining the relatively high initial porosity, coupled to the progressive melt consumption through melt-peridotite reaction during the percolation (*i.e.*, high extent of transient melt crystallisation), which is here simulated by the progressive increase of the crystallisation rate. As starting reacting melt, we used the REE composition of the liquid resulting after the first step, *i.e.*, the liquid with the lowest REE abundance in Figure 2a (see also Fig. 3). We performed the second step of the model by assuming initial and final crystallization of pyroxenes and garnet (four-phase calculation; 0.6 Opx, 0.2 Cpx, 0.2 Grt). The mode of crystallisation assemblage has been derived by the thermodynamic modelling of eclogite melt/peridotite interaction (Fig. S-5; Section S.4 of the Supplementary Material). Other calculations also include amphibole or phlogopite (five-phase calculation; see the crystallisation modes in the caption of Fig. S-6c,d: 0.5 Opx, 0.2 Cpx, 0.2 Grt, 0.1 Amp/Phl)). The highest LREE and MREE enrichment is produced by the fractional crystallisation of pyroxenes and garnet, whereas the involvement of amphibole or phlogopite results in a moderate REE increment (*c.f.* Fig. 2b and Fig. S-6c,d). REE partition coefficients for amphibole and phlogopite are from Ionov *et al*. (2002) and Corgne *et al*. (2018), respectively. Olivine is always the dissolving phase. Results in terms of liquid REE patterns are reported in Figure 2b and 3. They account for the REE gradient, *i.e.*, the overall increase of REE abundance and LREE-HREE fractionation (Ce_N/Yb_N), observed in the retrogressed Grt-websterite (now tremolitite) bulks within the first 30 m of peridotite.

S. 4 Thermodynamic modelling

Thermodynamic modelling shown in Figure S-5 is performed with the software package Perple_X (http://www.perplex.ethz.ch; Connolly, 2005), using the thermodynamic database of Holland and Powell (1998) revised in 2002 (hp02ver.dat), and the following solution models described in Holland and Powell (1998) (HP), Diener and Powell (2012) (DP), Holland and Powell (2003) (I1,HP), and White *et al*. (2014) (W): Gt(HP) for garnet, Opx(HP) for orthopyroxene, O(HP) for olivine, Omph(HP) for clinopyroxene, Chl(W) for chlorite, Sp(HP) for spinel, Pheng(HP) for white mica, Bio(HP) for phlogopite, Pl(I1,HP) for ternary feldspars, cAmph(DP) for amphibole. The equation of state of water is taken from Holland and Powell (1998). Aim of the modelling was to estimate the modal composition of Grt-websterites before the LP hydration event resulting from the interaction between Grt-peridotite and the eclogite leucosome at peak conditions (3 GPa, 750 °C). Results indicate that the volume proportions of the hybrid websterite at X = 0.2 weight fraction and $\log a_{H2O}$ = -0.2 are: Opx 43.66 %, Ol 25.05 %, Grt 11.61 %, Cpx 12.96 % and Phl 6.72 %. This modal composition, normalised without olivine, has been used to estimate the modal mineral composition crystallised in the Step2 of the geochemical model resulting in Figure 2b.

Supplementary Tables

Table S-1

Sample distance from the contact, mineral association, and microstructure of the studied profile. See Table S-2 for minerals generations. An Excel version of Table S-1, is available for download from the online version of this article at https://doi.org/10.7185/geochemlet.2305

Table S-2

Mineral parageneses reconstructed in Chl-peridotites and tremolitite layers of Borgo. The HP and LP-HT metamorphic event is from Pellegrino *et al.* (2020) and *Tumiati *et al.* (2018) respectively. An Excel version of Table S-2, is available for download from the online version of this article at https://doi.org/10.7185/geochemlet.2305

Table S-3

Bulk rock major (oxide wt. %) and trace elements (µg/g) composition. bdl = below detection limit. An Excel version of Table S-3, is available for download from the online version of this article at https://doi.org/10.7185/geochemlet.2305

Supplementary Figures

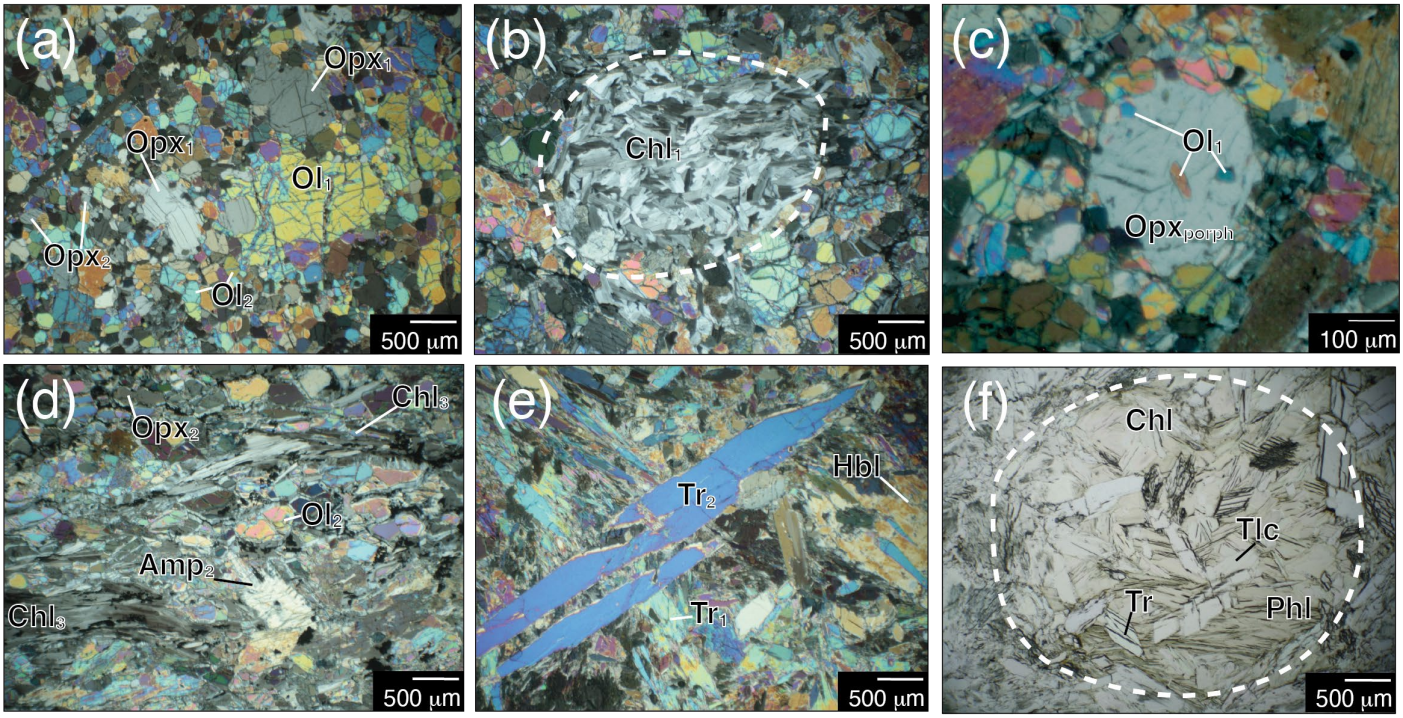

Figure S-1 Crossed polarised photomicrograph of retrogressed Grt-peridotite showing **(a)** two generations of Ol + Opx; **(b)** garnet completely substituted by chlorite (Chl_1); **(c)** metasomatic orthopyroxene (Opx_{porph}) growing at the expenses of olivine; **(d)** Amp_2 in equilibrium with Ol_2 and Opx_2 wrapped by a late-stage pervasive foliation of Chl_3. Crossed and plane polarised photomicrograph of retrogressed Grt-websterite (tremolitite) showing **(e)** relict Hbl overgrown by two Tr generations; **(f)** Phl + Chl + Tr + Tlc pseudomorph after garnet.

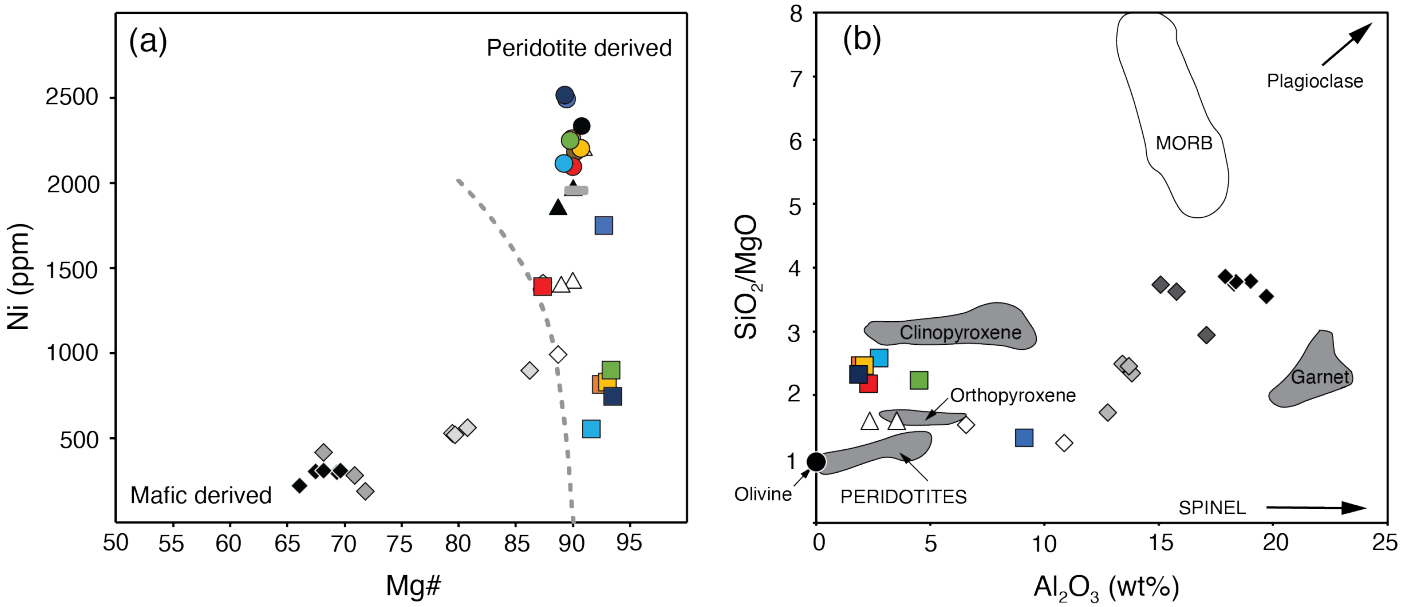

Figure S-2 (a) Mg# versus Ni plot of Chl-peridotite (coloured circles) and tremolitite (coloured squares) from Borgo (colours are the same as Fig. 3 and Fig. S-3). The dashed grey curve represents the possible transition from mafic to ultramafic derived rocks. **(b)** SiO_2/MgO versus Al_2O_3 of tremolitites from Borgo. The MORB array (white area) and the compositions of olivine (89% forsterite), orthopyroxene, clinopyroxene, and garnet in mafic rocks from orogenic peridotites (grey areas) are from Bodinier and Godard (2014) and references therein. Grt-peridotites from Mt. Duria (black triangles; Pellegrino *et al.*, 2020), Grt-pyroxenites (type A, black diamonds; type B, dark grey diamonds) and Sp-pyroxenites (type I, light grey diamonds; type II, white diamonds) from External Ligurides (Montanini *et al.*, 2012), UHP Grt-orthopyroxenites and websterites from Dabie Shan (white triangles; Malaspina *et al.*, 2006) and reference Depleted Mantle (grey solid line; Salters and Stracke, 2004) are also reported for comparison.

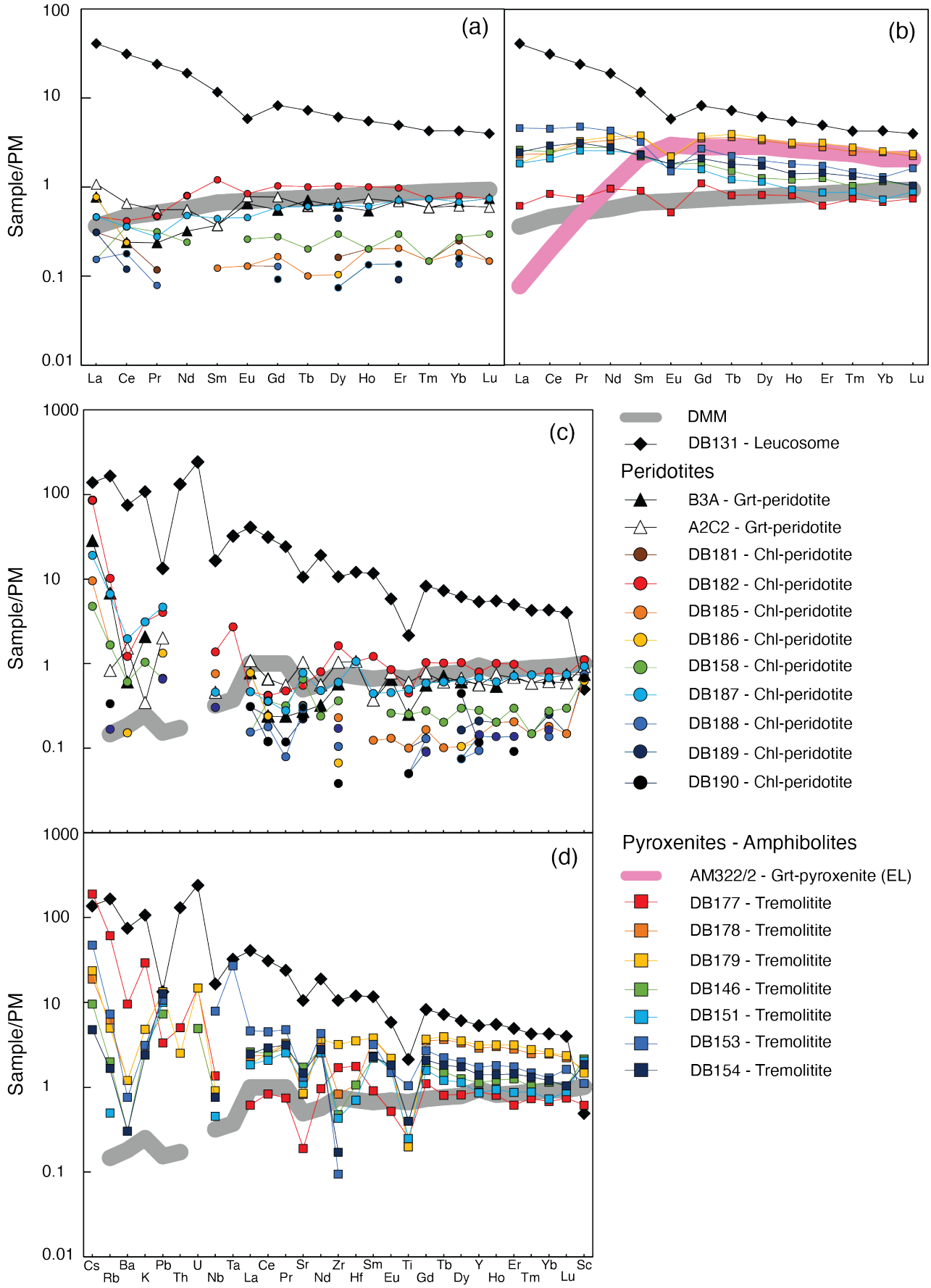
(a)
(b)
(c)
(d)
Sample/PM
100
10
1
0.1
0.01
1000
La Ce Pr Nd Sm Eu Gd Tb Dy Ho Er Tm Yb Lu
Cs Rb Ba K Pb Th U Nb Ta La Ce Pr Sr Nd Zr Hf Sm Eu Ti Gd Tb Dy Y Ho Er Tm Yb Lu Sc
DMM
DB131 - Leucosome
Peridotites
B3A - Grt-peridotite
A2C2 - Grt-peridotite
DB181 - Chl-peridotite
DB182 - Chl-peridotite
DB185 - Chl-peridotite
DB186 - Chl-peridotite
DB158 - Chl-peridotite
DB187 - Chl-peridotite
DB188 - Chl-peridotite
DB189 - Chl-peridotite
DB190 - Chl-peridotite
Pyroxenites - Amphibolites
AM322/2 - Grt-pyroxenite (EL)
DB177 - Tremolitite
DB178 - Tremolitite
DB179 - Tremolitite
DB146 - Tremolitite
DB151 - Tremolitite
DB153 - Tremolitite
DB154 - Tremolitite

Figure S-3 Primitive Mantle (PM) normalised REE and other trace element patterns of the investigated samples (data from Table S-3). Elements are presented in order of increasing compatibility (left to right) during melting in the upper mantle (Hofmann, 1988; Sun and McDonough, 1989). Normalising values are from McDonough and Sun (1995). **(a)** REE patterns of Grt-peridotites from Mt. Duria (triangles; Pellegrino *et al*., 2020) and Chl-peridotites from Borgo (coloured circles), compared with eclogite leucosome (black diamonds; Pellegrino *et al*., 2020) and reference Depleted MORB Mantle (grey solid line DMM; Salters and Stracke, 2004). **(b)** REE patterns of tremolitites from Borgo (coloured squares) compared with eclogite leucosome DB131 and Grt-pyroxenite from External Ligurides (EL, pink solid line AM322/2; Montanini *et al*., 2012). **(c, d)** Trace elements patterns of Grt-peridotites and tremolitites, respectively, compared with eclogite leucosome DB131 and DMM.

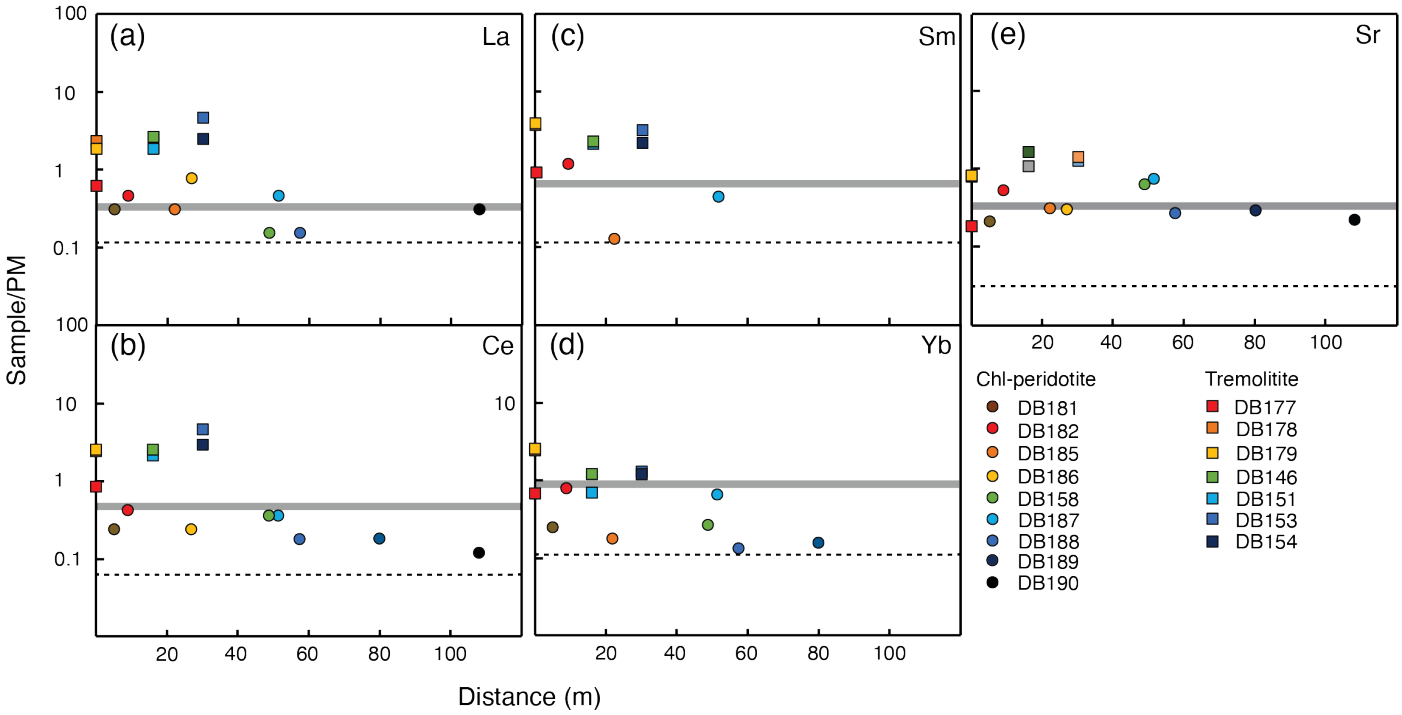

Figure S-4 Primitive Mantle normalised selected LREE **(a,b)** MREE **(c)** HREE **(d)** fluid mobile elements **(e)** of Chl-peridotites and tremolitites from Borgo along a 120 m length section starting from the contact with migmatised eclogites. The grey line is the reference DMM of Salters and Stracke (2004); the black dashed line is the analytical detection limit. Normalising values are from McDonough and Sun (1995).

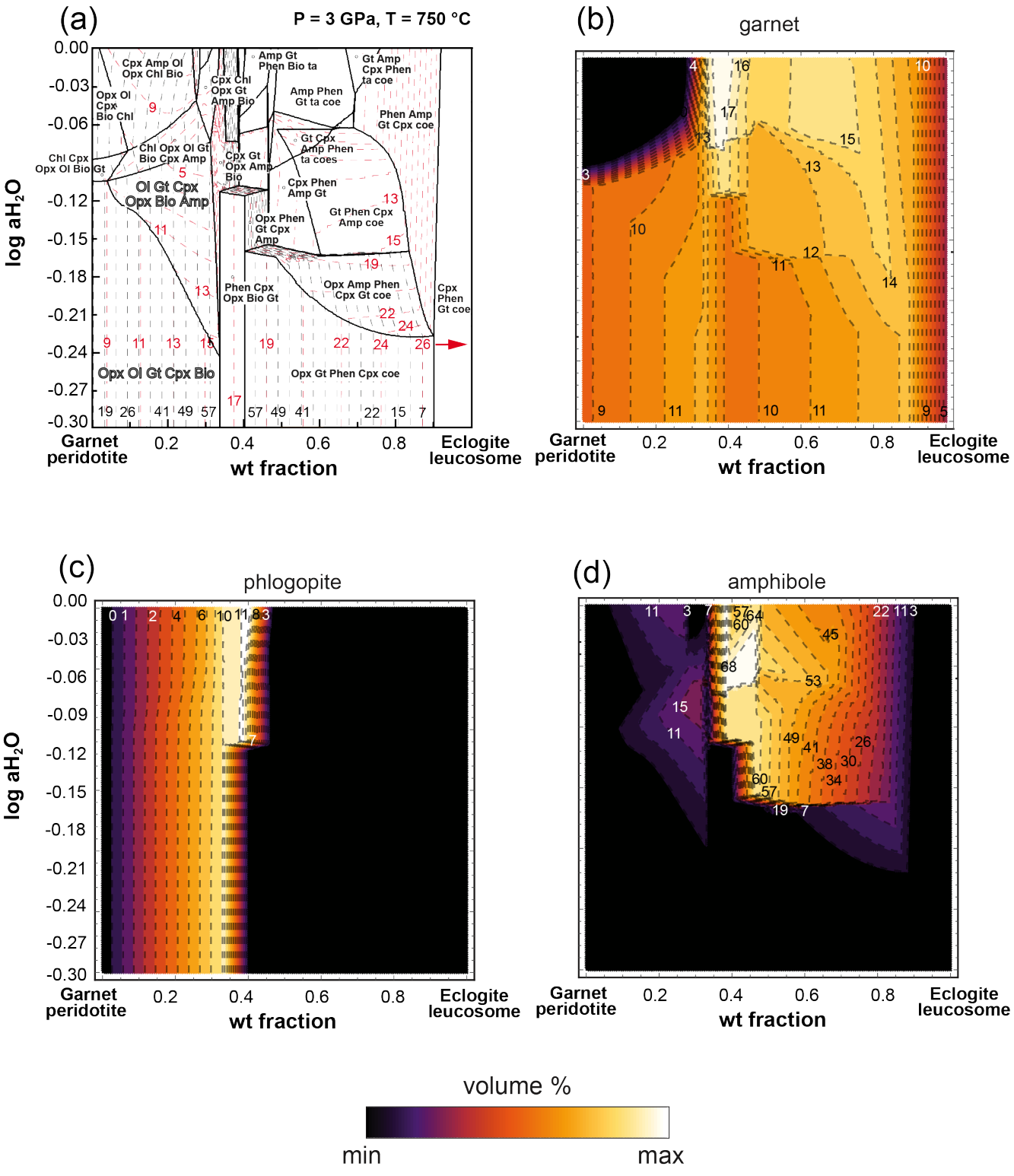
(a)
P = 3 GPa, T = 750 °C
log aH2O
wt fraction
Garnet peridotite
Eclogite leucosome
Cpx Amp Ol Opx Chl Bio
Amp Gt Phen Bio ta
Gt Amp Cpx Phen ta coe
Opx Ol Cpx Bio Chl
Cpx Chl Opx Gt Amp Bio
Amp Phen Gt ta coe
Phen Amp Gt Cpx coe
Chl Cpx Opx Ol Bio Gt
Chl Opx Ol Gt Bio Cpx Amp
Cpx Gt Opx Amp Bio
Gt Cpx Amp Phen ta coes
Ol Gt Cpx Opx Bio Amp
Cpx Phen Amp Gt
Gt Phen Cpx Amp coe
Opx Phen Gt Cpx Amp
Phen Cpx Opx Bio Gt
Opx Amp Phen Cpx Gt coe
Cpx Phen Gt coe
Opx Ol Gt Cpx Bio
Opx Gt Phen Cpx coe
(b)
garnet
(c)
phlogopite
(d)
amphibole
volume %
min
max

Figure S-5 (a) log aH_2O–X diagram calculated at fixed P = 3 GPa and T = 750 °C for garnet websterite forming after the melt-peridotite reaction. X = 0 corresponds to garnet peridotite (A2C2; Pellegrino *et al*., 2020), while X = 1 corresponds to the bulk of eclogite leucosome (DB131; Pellegrino *et al*., 2020). Dashed lines and corresponding numbers are the isomodes (vol%) of orthopyroxene (black) and clinopyroxene (red). **(b, c, d)** same log aH_2O–X diagram as shown in (a) reporting the isomodes (vol%) of garnet, phlogopite and amphibole respectively.

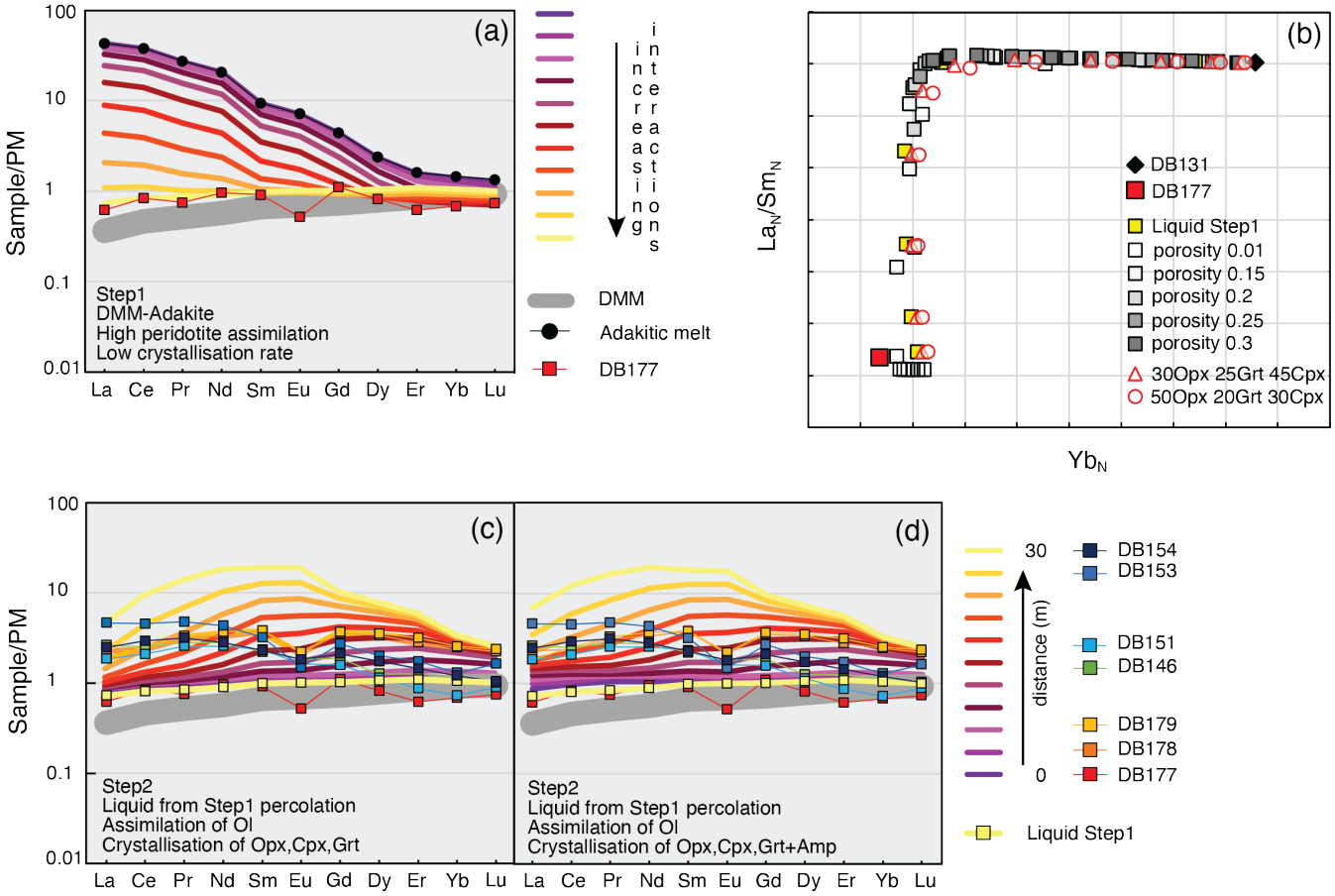

Figure S-6 Numerical simulation of melt-rock interaction at slab-mantle interface and reactive percolation of melt through mantle peridotite using Plate Model. **(a)** PM-normalised REE patterns of the liquid resulting from melt-peridotite interaction (Step1), using the same parameters as in Figure 2, but assuming as initial reacting melt the *adakite2* from Corgne *et al.* (2018). **(b)** PM-normalised Yb vs La/Sm of melt resulting from the percolation of the liquid after Step1 at variable porosity (squares) and 30% or 50% of orthopyroxene (triangles and circles) in the crystallizing assemblage. **(c, d)** Evolution of PM normalised REE abundances in the liquid originated by reactive percolation of reacted melt after Step1 through the DMM peridotite. Model assumes a high infiltrating melt amount (*i.e.*, starting porosity of 20%), low assimilation of olivine and high extent with the following modes: (c) 30% Cpx, 30% Opx and 40% Grt; (d) 50% Opx, 20% Cpx, 20% Grt and 10% Amp. Patterns with coloured squares (except light yellow) are the REE bulk compositions of tremolitites sampled in the Borgo outcrop within the first 30 meters from the migmatitic eclogite-peridotite contact (see Fig. 1). Coloured lines refer to the progressive cells of the model.

Supplementary Information References

Bodinier, J.L., Godard, M. (2014) Orogenic, Ophiolitic, and Abyssal Peridotites. *Treatise on Geochemistry (Second Edition)*, Elsevier, 2014, Pages 103-167. https://doi.org/10.1016/B978-0-08-095975-7.00204-7.

Connolly, J.A.D. (2005) Computation of phase equilibria by linear programming: A tool for geodynamic modeling and its application to subduction zone decarbonation. *Earth and Planetary Science Letters* 236, 524–541. https://doi.org/10.1016/j.epsl.2005.04.033

Corgne, A., Schilling, M.E., Grégoire, M., Langlade, J. (2018) Experimental constraints on metasomatism of mantle wedge peridotites by hybridized adakitic melts. *Lithos 308*, 213-226. https://doi.org/10.1016/j.lithos.2018.03.006

Diener, J.F.A., Powell, R. (2012) Revised activity-composition models for clinopyroxene and amphibole. *Journal of Metamorphic Geology* 30, 131–142. https://doi.org/10.1111/j.1525-1314.2011.00959.x

Hofmann, A.W. (1988) Chemical differentiation of the Earth: the relationship between mantle, continental crust and oceanic crust. *Earth and Planetary Science Letters* 90, 297–314. https://doi.org/10.1016/0012-821X(88)90132-X

Holland, T.J.B, Powell, R. (1998) An internally consistent thermodynamic data set for phases of petrological interest. *Journal of Metamorphic Geology* 16, 309-343. https://doi.org/10.1111/j.1525-1314.1998.00140.x

Holland, T.J.B., Powell, R. (2003) Activity–composition relations for phases in petrological calculations: an asymmetric multicomponent formulation. *Contributions to Mineralogy and Petrology* 145, 492–501. https://doi.org/10.1007/s00410-003-0464-z

Ionov, D.A., Bodinier, J.L., Mukasa, S.B., Zanetti, A. (2002) Mechanisms and sources of mantle metasomatism: major and trace element conditions of peridotite xenoliths from Spitzbergen in the context of numerical modelling. *Journal of Petrology* 43, 2219–2259. https://doi.org/10.1093/petrology/43.12.2219

Malaspina, N., Hermann, J., Scambelluri, M., Compagnoni, R. (2006) Polyphase inclusions in garnet-orthopyroxenite (Dabie-Shan, China) as monitors for metasomatism and fluid-related trace element transfer in subduction zone peridotite. *Earth and Planetary Science Letters* 249, 173–187. https://doi.org/10.1016/j.epsl.2006.07.017

McDonough, W.F., Sun, S.S. (1995) Composition of the Earth. *Chemical Geology* 120, 223–253. https://doi.org/10.1016/0009-2541(94)00140-4

Montanini, A., Tribuzio, R., Thirlwall, M. (2012) Garnet clinopyroxenite layers from the mantle sequences of the Northern Apennine ophiolites (Italy): Evidence for recycling of crustal material. *Earth and Planetary Science Letters* 351-352, 171–181. https://doi.org/10.1016/j.epsl.2012.07.033

Pellegrino, L., Malaspina, N., Zanchetta, S., Langone, A., Tumiati, S. (2020) High pressure melting of eclogites and metasomatism of garnet peridotites from Monte Duria Area (Central Alps, N Italy): A proxy for melt-rock reaction during subduction. *Lithos* 358-359, 105391. https://doi.org/10.1016/j.lithos.2020.105391

Pertermann, M., Hirschmann, M. M. (2003) Anhydrous partial melting experiments on MORB-like eclogite: phase relations, phase compositions and mineral–melt partitioning of major elements at 2–3 GPa. *Journal of Petrology* 44, 2173-220. https://doi.org/10.1093/petrology/egg074

Rapp, R.P., Norman, M.D., Laporte, D., Yaxley, G.M., Martin, H., Foley, S.F. (2010) Continent formation in the Archean and chemical evolution of the cratonic lithosphere: melt–rock reaction experiments at 3–4 GPa and petrogenesis of Archean Mg-diorites (sanukitoids). *Journal of Petrology* 51, 1237-1266. https://doi.org/10.1093/petrology/egq017

Salters, V.J.M., Longhi, J.M., Bizimis, M. (2002) Near mantle solidus trace element partitioning at pressures up to 3.4 GPa. *Geochemistry, Geophysics, Geosystems* 3, 1-23. https://doi.org/10.1029/2001GC000148

Salters, V.J.M., Stracke, A. (2004) Composition of the depleted mantle. *Geochemistry Geophysics Geosystems* 5. https://doi.org/10.1029/2003GC000597

Sun, S.S., McDonough, W.F. (1989) Magmatism in Ocean Basins Chemical and Isotopic Systematics of Ocean Basalts: Implications for Mantle Composition and Processes. *Geological Society of London, Special Publications* 42, 313-345. https://doi.org/10.1144/GSL.SP.1989.042.01.19

Tumiati, S., Zanchetta, S., Pellegrino, L., Ferrario, C., Casartelli, S., Malaspina, N. (2018) Granulite-facies overprint in garnet peridotites and kyanite eclogites of Monte Duria (Central Alps, Italy): clues from srilankite-and sapphirine-bearing symplectites. *Journal of Petrology* 59, 115-151. https://doi.org/10.1093/petrology/egy021

Vernières, J., Godard, M., Bodinier, J.L. (1997) A plate model for the simulation of trace element fractionation during partial melting and magma transport in the Earth's upper mantle. *Journal of Geophysical Research: Solid Earth*, 102, 24771-24784. https://doi.org/10.1029/97JB01946

Wang, C., Cascio, M.L., Liang, Y., & Xu, W. (2020) An experimental study of peridotite dissolution in eclogite-derived melts: implications for styles of melt-rock interaction in lithospheric mantle beneath the North China Craton. *Geochimica et Cosmochimica Acta* 278, 157-176. https://doi.org/10.1016/j.gca.2019.09.022

White, R.W., Powell, R., Johnson, E. (2014) The effect of Mn on mineral stability in metapelites revisited: New a–x relations for manganese-bearing minerals. *Journal of Metamorphic Geology* 16, 309-343. https://doi.org/10.1111/jmg.12095